Journal of Microwaves, Optoelectronics and Electromagnetic Applications, Vol. 22, No. 4, December 2023
DOI: http://dx.doi.org/10.1590/2179-10742023v22i4273046

kHz Linewidth Laser Characterization using Low Frequency and Excess Noise Measurements

Seyed Saman Mahjour[1], Mareli Rodigheri[1], Cristiano M Gallep[2], Evandro Conforti[1]*
[1]*School of Electrical and Computer Engineering, University of Campinas, Campinas, Sao Paulo, Brazil.*
[2]*School of Technology, University of Campinas, Limeira, Sao Paulo, Brazil.*
*Corresponding author: mareli@decom.fee.unicamp.br (Mareli Rodigheri)

***Abstract*— Low frequency noise (LFN) of highly coherent laser (linewidth below 10 kHz) is analyzed using an unbalanced Mach-Zehnder interferometer (UMZI) with adjustable long arm span. Furthermore, the Laser Relative Excess Noise (LREN) is introduced here to set a comparison of the laser coherence in relation to its emission power. The LREN is obtained using the addition of laser high and low frequency noises that appear in excess to the ideal power spectral density (PSD) Lorentzian distribution. Using this approach, it is possible to compare the tested laser in relation to an ideal laser with the same linewidth.**

Index Terms—laser excess noise, laser linewidth, laser low frequency noise, unbalanced Mach-Zehnder interferometer.

I. Introduction

Long lifetime, small size, monolithic integration, and selectable wavelength are among the laser diodes (LD) achievements [1], [2]. The LD technical improvements have been supported by physical modeling, including sophisticated numerical analyzes [3]. The experimental device characterization includes double heterojunction LDs [4], quantum well LDs [1], quantum dot LDs [5], external cavity lasers (ECL) [6], integrated external cavity lasers [6], [7], and below kHz linewidth lasers [6]. Specifically for optical communications, stable and narrower linewidth lasers - possibly ranging below kHz - are desired for optimal detection of optical carriers when using multilevel/phase modulation [8]. The narrow linewidth reduces the complexity of post-detection digital signal processing (DSP) circuits, specifically in short-distance optical fiber systems (few km range) such as data centers [6], [8]. The obtained improvements include output power enhancement, decrease in threshold currents [4], high electro-optical conversion efficiency [1], and stable wavelength operation [9]. Nowadays, research efforts are focused on the reliability of high-power semiconductor LDs, their lifetime, power enhancement, and energy efficiency [4]. Investigations into the noise characteristics can also aid in the development of laser diodes with optimum performance, including the knowledge of the physical processes occurring inside the device [10].

Noise measurements can be used as a diagnostic tool to assess the reliability and stability of such devices. The low-frequency noise (LFN) data is important to evaluate the LD performance [10] and is a potential tool for nondestructive laser quality assessment [4]. Most LD failures are caused by numerous defects and imperfections introduced throughout the manufacturing process. The LFN components such as the $1/f$ noise, are extremely sensitive to any imperfections in the laser structure. The $1/f$ noise can change the PSD Lorentzian pattern into a Voigt curve [11]. There is a correlation between the

Brazilian Microwave and Optoelectronics Society-SBMO *received 17 Mar 2023; for review 19 Apr 2023; accepted 05 Oct 2023*
Brazilian Society of Electromagnetism-SBMag *ISSN 2179-1074*

LFN intensity fluctuations and the frequency fluctuations of the optical emission [12]. The $1/f$ noise is converted into phase noise through the material nonlinearities and might degrade the LD purity, increasing its linewidth [13], [14]. Optoelectronic devices are part of this process, such as any electronic device involved in the link [15]. This paper proposes an approach for using the LNF measurement as an effective and non-destructive testing technique to analyze the LD quality.

It is possible to study the internal defect in LDs by analyzing its LFN characteristics [4]. Some factors like internal defects, surface damage, and leakage currents might cause the capture and release of electrical carriers in a stochastic manner by the interface traps, resulting in tiny current fluctuations [16], [17]. The measured LFN can indicate internal defects in the active region and can be used to assess the device performance, including the lifetime of a semiconductor laser [4]. Therefore, the LFN measurement can be used as an effective, nondestructive testing method to assess the property and reliability of LD [10], [18]. Electric aging tests, as a traditional and destructive examination method, are commonly used to assess the reliability of diode lasers [19]. Long-term testing under high currents, particularly for high-power semiconductor laser diodes, can damage the active region and severely harm the internal structure. As a result, it is important to investigate a non-destructive testing process [4]. It is experimentally demonstrated that the increase in the residual spectral linewidth during LD degradation is due to an increase in the $1/f$ noise. Also, the increase in spectral linewidth is related to buried heterostructure (BH) interface degradation [20]. As the LD degradation proceeds, the linewidth gradually increases, and the residual linewidth also increases. The residual linewidth is determined by the $1/f$ noise. Thus, it can degrade the data transmission rate and increase the bit-error rate [21].

Laser's light includes a variety of noises such as the shot noise [22], the thermal noise [23], the generation-recombination noise [24], the spontaneous emission noise [22] and the $1/f$ noise [25]. The overall consequences of these noise sources are variations in laser intensity, phase, and optical frequency, even when the laser is biased at a constant bias with minor current fluctuations. When LDs are operated at constant current, intensity fluctuations result in a limited signal-to-noise ratio (SNR), whilst phase variations result in a finite spectral linewidth. Since such variations can impact the performance of lightwave systems, it is essential to determine their magnitude [22]. The term "laser noise" refers to the random fluctuations of various output parameters, including amplitude, phase, and polarization [26]. This is a common issue that has a significant impact on many applications in photonics, particularly on precise measurements. In the context of lasers, fluctuation parameters refer to the various factors that can cause fluctuations or variations in the laser output. These fluctuations can manifest as laser noise, which can have implications for various applications of lasers. Power Fluctuations is the variations in the output power of the laser can lead to laser noise. For example, if the laser output power fluctuates significantly over time, it can cause instability in measurements or impair the performance of laser-based systems. Frequency Fluctuations is the changes in the laser's output frequency or wavelength can cause fluctuations in the optical phase, leading to phase noise. This is particularly important in applications that require precise frequency stability, such as optical communication systems and laser interferometry. Amplitude Fluctuations is the random fluctuations in the amplitude of the laser output can result in amplitude noise. This can affect applications such as laser spectroscopy or imaging where a stable and consistent amplitude is crucial. Consider, for example, interferometric position measurements, which can be directly influenced by optical phase fluctuations, or spectroscopic transmission measurements, where intensity variations limit the achievable sensitivity [27]. Similarly, all those optical noises limit

Brazilian Microwave and Optoelectronics Society-SBMO *received 17 Mar 2023; for review 19 Apr 2023; accepted 05 Oct 2023*
Brazilian Society of Electromagnetism-SBMag *ISSN 2179-1074*

the data rate and the transmission distance of fiber-optic systems [8], [28].

Phase noise is defined as variations in the phase of the output optical carrier. Due to various influences, even a single-frequency laser will not produce a perfectly sinusoidal electric field oscillation at its output since it always includes some intensity or phase fluctuations [26]. The observed linewidth is due to the spectral broadening caused by phase variations [24]. The laser linewidth is strongly connected to the phase noise; however, the laser linewidth conveys far less information than the entire phase noise spectrum [26]. The intensity and phase of the optical field are affected by quantum fluctuations associated with the lasing process [24].

The injected bias current can be a source of LFN noise due to the generation and recombination of charged carriers [29]. So, the noisier the injected bias current, the noisier the LD light stream [30]. Electrical noise and optical fluctuations have a cross-correlation [14], [30]. Carrier mobility fluctuations cause fluctuations in the voltage across the intrinsic region. Subsequently, it can enhance the LFN in homogeneous semiconductor lasers [31]. Biasing any semiconductor heterojunction intrinsically produces carrier density fluctuations. These fluctuations will therefore induce fluctuations in the refraction index n and absorption factor α, altering the emitted frequency and the amplitude noises. The LFN noise is originated so in carrier density fluctuations and also in absorption fluctuations [32].

Moreover, heterojunction interface degradation can cause laser degradation as well: the quality of the heterojunction interface affects the LFN [33], [34]. As the heterojunction interface degradation continues, some kinds of defects increase at the heterojunction interface [21]. These defects cause an increase in the interfacial recombination rate, followed also by a rise in the nonradiative recombination and, finally, in the LFN. The increase in LFN results in the rise of residual linewidth and the bias threshold. Residual linewidth is an important concern in such lasers, determining the minimum linewidth at high output power [21], [24], [35]. It can be concluded that there is a strong relation between LFN increase and device degradation [36]. Therefore, by analyzing the LFN noise characteristics it is possible to study the impact of internal defects in LDs [4]. The measured LFN can so be used to assess the device performance and lifetime of the semiconductor lasers [4]. Therefore, the LFN measurement can be used as an effective nondestructive testing method to assess the property and reliability [10], [18].

In this work the LFN and high-frequency excess noise of highly coherent laser (linewidth below 10 kHz) is analyzed using an unbalanced Mach-Zehnder interferometer (UMZI) with an adjustable long arm span. Furthermore, the Laser Relative Excess Noise (LREN) is introduced here to set a comparison of the laser coherence in relation to its emission power. The LREN is obtained using the laser low and high-frequency excess noise in relation to the ideal power spectral density (PSD) Lorentzian distribution.

II. Experimental Setup

In the heterodyne technique, the frequency of the optical input signal is converted down to the radiofrequency (RF) range by mixing with a local oscillator during coherent detection [37]. The requirement for a local oscillator is eliminated in the self-homodyne technique, in which the optical signal is combined with a delayed version of itself. The UMZI has the advantages of being a simple structure, with a large measuring range and minimal optical transmission loss [38]. However, because the beating center frequency ν_b is 0 Hz, low-frequency noise sources in the environment might interfere with the results. Given the sensing characteristics of the optical fiber, the environmental acoustic noise

Brazilian Microwave and Optoelectronics Society-SBMO *received 17 Mar 2023; for review 19 Apr 2023; accepted 05 Oct 2023*
Brazilian Society of Electromagnetism-SBMag *ISSN 2179-1074*

and temperature, pressure variations, and other factors can have a significant impact on the test results [38], [39].

The UMZI setup, shown in Fig. 1, consists of two directional couplers connected by two delay lines of different lengths [6], [40]. The self-homodyne method is an interferometric technique for measuring optical carrier linewidth using power spectral density (PSD). The PSD results from the beat between the signal and a delayed portion of the same signal. With this beat signal, its phase fluctuation $\phi(t)$ is retrieved as a variation of the current intensity after the square photodetector and transformed into the power spectral density using a spectrum analyzer [40]. In this interferometer, where one arm is much longer than the other, the imbalance causes a relative time delay, τ_{DL}, in such a way to break the phase coherence between the direct and delayed signals. Consequently, when the mixed signals are detected by a photodetector, the electrical spectrum measured after photodetection is an indicator of laser phase noise [39].

In the configuration shown in Fig. 1, the optical carrier of the laser under test is split into two paths by a $50:50$ beam splitter. The optical carrier in one path is delayed by a time interval relative to the other path. The longer arm has a standard optical fiber spool, ranging from 60m to 100 km. This difference in length between the two arms results in a time delay, denoted τ_{DL}, which ranges from 0.3 μs to 500 μs. Thus, the optical signals in the two MZI arms could lose phase coherence when $\tau_{DL}/\tau_C >> 1$, where τ_C is the laser coherence time. This scenario is commonly referred to as a non-coherent regime.

The short arm has an adjustable optical polarization control (PC) that provides polarization matching with the other wavefront. However, the state of polarization (SOP) may drift randomly due to the fiber birefringence effect and cannot be fully controlled by PC, resulting in some instability in the detected self-homodyne spectrum and so in linewidth measurement errors.

There are some techniques to make it possible to consider a polarization measurement at the spool inlet and outlet in order to mitigate the random polarization variations and minimize the resulting linewidth measurement errors in a self-homodyne interferometer. By monitoring the state of polarization (SOP) at both ends of the spool, and one can effectively characterize and compensate for any changes in polarization introduced by fiber birefringence effects. Techniques includes Polarization Measurement at Inlet and Outlet, by installing polarization measurement devices, such as polarization analyzers, at the spool's inlet and outlet. These devices can analyze the SOP of the optical signal at each location. Another way is Characterize Polarization Drift, by continuously monitor the SOP at both ends of the spool over time. This will allow you to observe any random polarization variations or drift caused by fiber birefringence. Feedback Control is the other technique, using the polarization measurement results to provide feedback control to the system. If a significant change in SOP is detected, appropriate corrective actions can be taken to stabilize the polarization. This can involve adjusting the polarization controller

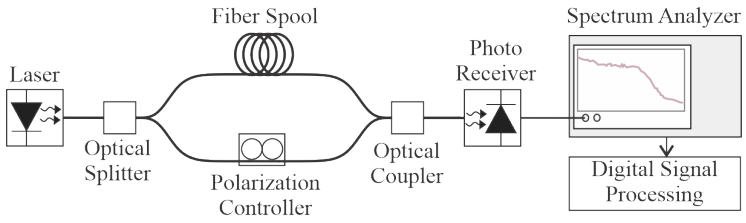

Fig. 1. The experimental set-up for linewidth measurement using the self-homodyne method.

  ISSN 2179-1074

(PC) or implementing polarization compensation techniques to counteract the effects of birefringence. Compensation Techniques and PSD Result Stabilization are the other alternative techniques.

On practical situations, many beat frequency signals are observed due to fluctuations in the laser wavelength. To measure the low frequency range, one requires a long delay fiber, typically more than 10 km. However, the accuracy of the LFN measurements are influenced by several aspects such as the noise due to the laser bias source, the polarization mismatch, the 1/f frequency noise intensity, the Stimulated Brillouin scattering (SBS) effect and also environmental factors such as temperature and vibration [6].

To adjust the polarization in our experiment, we utilized a method that allows for a more precise polarization adjustment. The optical polarization controller must be carefully adjusted, therefore, by using time-domain analysis (oscilloscope mode of ESA, in this case), it is possible to obtain the best possible mixed signal and ultimately the maximum power in the spectrum analyzer. When the optical carriers in the two interferometer arms mix at the second coupler they interact constructively (add up) and destructively (cancel out) accordingly to their polarization (mis)match. If the polarization of the optical carrier coming from the short arm signal is orthogonal to the one from the long arm signal, the interference will be zero and they will annihilate each other, resulting in the worst PSD. The polarization adjustment is presented in Fig. 2, with Fig. 2a, c, e and g showing the oscilloscope mode and Fig. 2b, d, f and h the correspondent resonance peak. In this scenario, a large resonance peak is visible as a result of poor PC optimization (see point X in Fig. 2b). When the optical carriers mix at the same polarization, they add up constructively and we get the maximum power in PSD data, and the noise properly shows the Gaussian and Lorentzian profiles, as shown in (Fig. 2h). In this scenario, the X point has disappeared, indicating that the PC adjustment has been finely tuned and that the best measurement for laser linewidth may be obtained with this adjustment. This resonance is similarly observed in our group's previous study [6]. In that experiment a HeNe laser with linewidth ≈ 750Hz presented such resonance at ≈ 18Hz, similarly to what is shown now for semiconductor lasers [6]. This resonance is highly dependent on the Polarization Control adjustment; however, other factors such as laser power and delay fiber length have an effect on the size of the resonance.

After that, the two optical paths combine through another $50:50$ beam splitter, and carriers are mixed after proper polarization optimization and further coupled to a photodiode. The amplitude of the signal is measured here by an 100 kHz Electrical Spectrum Analyzer (ESA, HP3561A) and the signal power spectrum density is obtained by the Fourier transform of the signal autocorrelation function. The electrical spectrum analyzer was connected to a computer by USB/GPIB interface and the data was acquired by software (HP7470A plotter emulator).

According to Schawlow–Townes equation which represented in Eq. 1 for measuring the laser linewidth [6], [39], [41]

$$\Delta\nu_{laser} = \frac{4\pi h\nu(\Delta\nu_c)^2}{P_{out}} \tag{1}$$

where $\Delta\nu_{laser}$ is the theoretical laser linewidth (Lorentzian lineshape), P_{out} is the laser emitted power, $h\nu$ is the emitted photon energy, ν is the laser optical central emission frequency in the laser spectrum (assuming a quasi-monochromatic wave), h is the plank constant, $\Delta\nu_c$ is the resonator cavity bandwidth and τ_c is the coherent time of the laser. We consider here only monomode lasers with a Lorentzian

Brazilian Microwave and Optoelectronics Society-SBMO *received 17 Mar 2023; for review 19 Apr 2023; accepted 05 Oct 2023*
Brazilian Society of Electromagnetism-SBMag *ISSN 2179-1074*

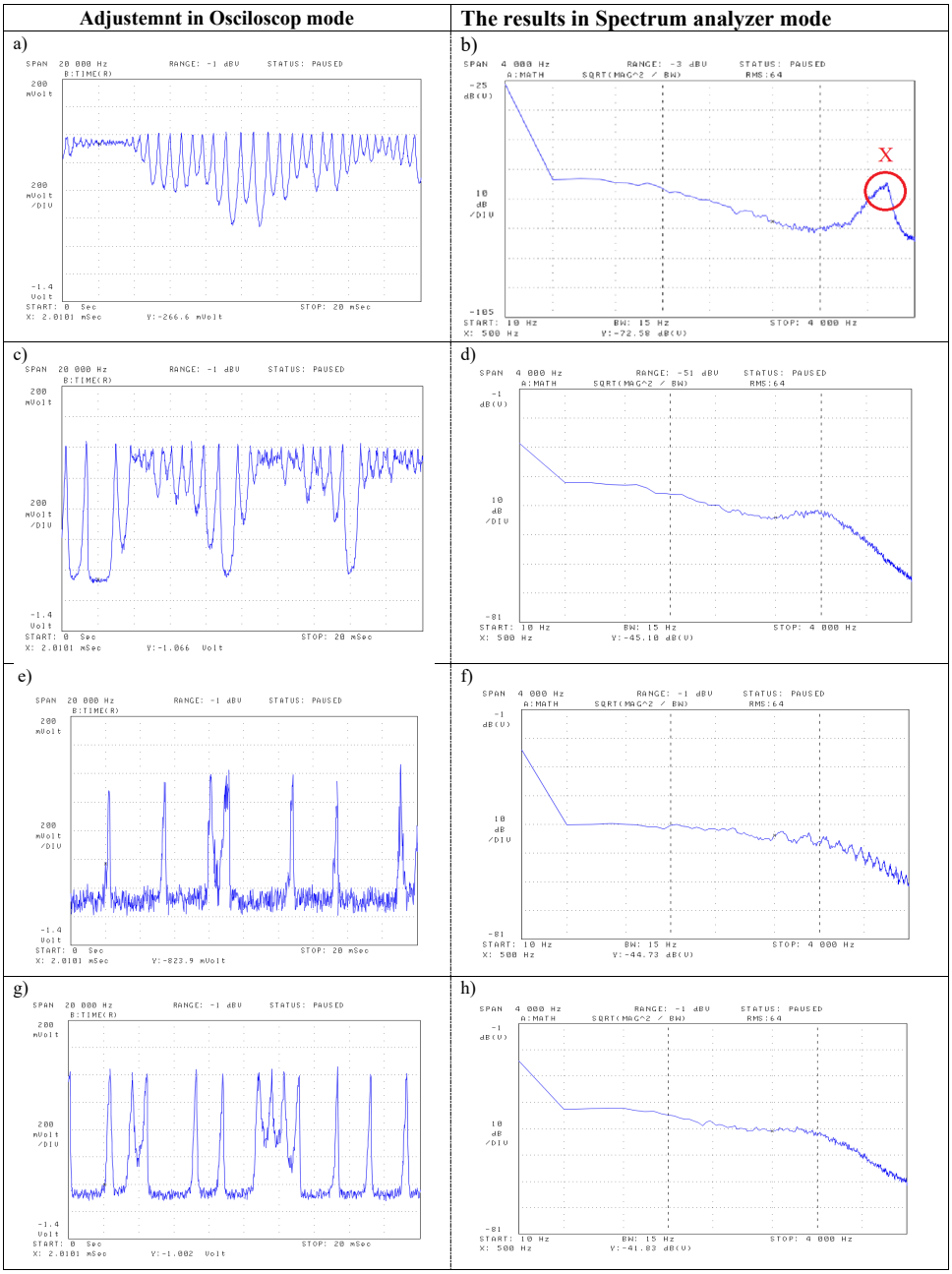

Fig. 2. The different effects of polarization control adjustment on the PSD results in terms of the obtaining beat signals. a) The worst adjustment: The polarization of the signals in two arms are almost perpendicular to each other therefore they cancel out each other. b) The worst result: a minimum power is obtained in the PSD and there is a big surge (point X) in the curve. c) Bad adjustment: Beat frequency signals are poorly obtained since the polarization control is not adjusted properly. d) Bad result: Because the polarization control has not been appropriately tuned, the noise power spectrum density is poor and it does not contain the maximum power, however the X point decreases dramatically. e) Without adjustment: the beat signal is not Sharpley observable due to no PC adjustment. f) There are many oscillations in the spectrum. g) The best adjustment: the beating signal is sharply obtained since the PC is well adjusted. h) The best result: noise power spectrum density is obtained as a result of proper OPC adjustment.

spectrum [34], [35]. Therefore, the laser Lorentzian linewidth $\Delta\nu_L$ is given by:

$$\Delta\nu_L \approx \frac{1}{\pi\tau_c} \tag{2}$$

The experimental setup (see Fig. 1). The self-homodyne interferometer is configured to investigate the spectral component of the intrinsic noises of an Integrated External Cavity laser (IECL, manufactured by Redfern Integrated Ooptics Inc.) with variable fiber spool with a delay length L, and laser power P.

The analyzes used an algorithm developed in MATLAB to obtain the data and to process the results. The data for different laser powers and optical fiber lengths were acquired from the Spectrum Analyzer; following steps, calculations were performed to convert the noise PSD unit and to conform the signal vector to the algorithm theoretical Lorentzian fittings. The bandwidth of the half-spectrum (FWHM - Full Width at Half Maximum) of the laser under test is derived as a result of this adjustment. A Gaussian adjustment was also considered for modeling the noise at low frequencies. Eq. 3 and Eq. 4 were used to fit Lorentzian and Gaussian curves, respectively:

$$L(f) = k_L . \frac{\frac{\Delta_\nu}{2}}{f^2 + \left(\frac{\Delta_\nu}{2}\right)^2} \tag{3}$$

$$G(f) = \frac{k_G}{\sigma\sqrt{2\pi}} . exp\left(\frac{-f^2}{2\sigma^2}\right) \tag{4}$$

where k_L and k_G are constants, σ is the standard deviation of Gaussian noise, and Δ_ν is the FWHM linewidth.

Finally, the theoretical fitting curves are used to calculate the percentage of power contained in each of the three major regions of the PSD spectrum. These three parts are Low Frequency Phase Noise (LFPN), P_G, which has the Gaussian spectrum, White Phase Noise (WPN), P_L, has the Lorentzian spectrum. Also, the High Frequency Excess Phase Noise (HFEPN) appeared in the experimental PSD and is named P_E. The total photodetected PSD power is, P_T. As a result, the discrete integrals in Eq. 5, Eq. 6 and Eq. 7 are developed.

$$P_L = \sum_{f=0}^{n} L(f).\Delta f \tag{5}$$

$$P_G = \sum_{f=0}^{n} G(f).\Delta f \tag{6}$$

$$P_T = \sum_{f=0}^{n} PSD(f).\Delta f \tag{7}$$

The term Δf in Eq. 5 to Eq. 7 describes the width of the rectangle in the integration of the PSD, or, in the physical sense, the frequency spacing between two subsequent points. $PSD(f)$ in Eq. 7 represents the experimental spectral points acquired at each frequency f. The n value is the frequency span, and 100 kHz was used here. It is worth noting that HFEPN is given by $P_E = P_T - P_L - P_G$.

Based on the PSD power analyzes presented here, the Laser Relative Excess Noise (LREN) is proposed to evaluate both low frequency and high frequency noises. So, the LREN is defined as the ratio between the overall laser noises power outside the Lorentzian spectrum and the power inside the Lorentzian fitting of the PSD, as shown in Eq. 8.

$$LREN = \frac{P_E + P_G}{P_L} \tag{8}$$

Brazilian Microwave and Optoelectronics Society-SBMO *received 17 Mar 2023; for review 19 Apr 2023; accepted 05 Oct 2023*
Brazilian Society of Electromagnetism-SBMag *ISSN 2179-1074*

This metric provides a comprehensive evaluation of noise levels across different frequency ranges, allowing for a more accurate assessment of laser performance. By calculating the LREN value using this equation, laser researchers and engineers can effectively quantify the extent of excess noise present in the laser system. This information is crucial for optimizing laser performance, identifying potential sources of noise, and making informed decisions regarding noise reduction strategies in various applications, such as optical communication, precision measurements, and laser-based sensing technologies. The LREN metric provides a standardized and reliable approach to assess and compare different lasers' noise characteristics, aiding advancements in laser technology and its diverse applications.

III. Results

The results for two IECL tested here (RIO1 and RIO2) are presented in two forms: Double Side Band (DSB) and Single Side Band (SSB), as shown respectively at Fig. 3a and Fig. 3b, where the Lorentzian and Gaussian fittings were applied to analyze the PSD.

We discovered early on in our research that the Lorentzian curve did not work well for fitting the first few hundred hertz. As a result, we used a Gaussian noise model for frequencies up to 450 Hz. We used a Lorentzian curve for the remaining spectrum, which is frequently connected to phase noise from spontaneous photon emission. As a result, both fits are useful for examining the LFN spectrum.

However, for the second remaining part of spectrum (above the 450 Hz) we used a Lorentzian curve. In the context of low-frequency noise measurement in an unbalanced Mach-Zehnder interferometer, a Lorentzian fit is often preferred over a Gaussian fit for several reasons. First, the nature of Low-Frequency Noise, typically exhibits characteristics that align more closely with a Lorentzian distribution rather than a Gaussian distribution. Lorentzian noise is characterized by a slower roll-off at low frequencies, which better represents the behavior of low-frequency noise sources commonly found in optical systems, such as thermal noise and flicker noise. Second, Power Spectral Density (PSD) Representation. The power spectral density is commonly used to represent noise in frequency domain analysis. In the case of low-frequency noise, the PSD plot often exhibits a 1/f characteristic, where the noise power decreases inversely with frequency. A Lorentzian fit aligns with this 1/f behavior, providing a more accurate representation of the noise spectrum at low frequencies. The other reason is noise Component Separation, in many optical systems, low-frequency noise may coexist with other

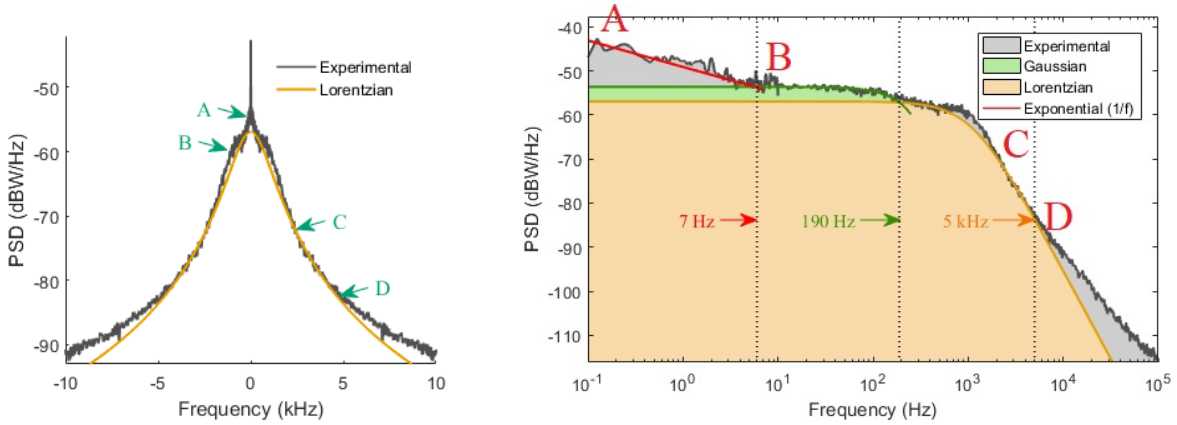

(a) Points of interest

(b) Relationship between the parts of the spectrum.

Fig. 3. Experimental result evaluating spectrum (for RIO1 laser).

Brazilian Microwave and Optoelectronics Society-SBMO *received 17 Mar 2023; for review 19 Apr 2023; accepted 05 Oct 2023*
Brazilian Society of Electromagnetism-SBMag

ISSN 2179-1074

noise components, such as white noise or high-frequency noise. A Lorentzian fit allows for better separation and characterization of the low-frequency noise component, enabling more precise analysis and understanding of the system's noise behavior. Last but not least, Physical Interpretation. The Lorentzian distribution has a clear physical interpretation in the context of low-frequency noise. It is associated with relaxation processes, such as the time constant of a resonator or the characteristic time of a physical system. This makes the Lorentzian fit more intuitive and meaningful when trying to understand the underlying noise mechanisms in the system. While Gaussian fits are commonly used for many noise distributions, a Lorentzian fit is often preferred for low-frequency noise analysis in an unbalanced Mach-Zehnder interferometer due to its better alignment with the nature of low-frequency noise, the characteristics of the PSD plot, the ability to separate noise components, and its physical interpretation.

To conduct the investigation, we utilized the interferometer setup discussed earlier. The frequency range under investigation spans from 0 to 100 kHz, and it was divided into decades to improve resolution at lower frequencies. We performed a series of experiments, each focusing on a specific frequency range. The first experiment covered the range from 0 Hz to 10 Hz, with a resolution of 0.025 Hz. Subsequently, the second experiment extended from 0 Hz to 100 Hz, with a resolution of 0.25 Hz, and so on. By combining the results from all five experiments, we constructed a comprehensive spectrum of the laser's noise characteristics. To ensure coherent operation during the experiments, we took care to configure the setup properly. Specifically, we ensured that the delay time introduced by the fiber spool, represented as τ, remained shorter than the coherence time of the optical source, denoted as τ_c. This step is crucial because if the delay time is excessively long (resulting from a long fiber spool), it could introduce additional noise, such as 1/f noise [8]. After gathering the necessary data, we subjected it to analysis using a subsequent algorithm, which will be elaborated upon in the following sections.

We conducted an analysis of the noise present in the experimental measurements using theoretical Gaussian and Lorentzian models, along with calculating their respective areas. To accomplish this, we combined different segments with matching power and fiber length, constructing a spectrum ranging from 0 Hz to 100 kHz, as illustrated in Fig. 3b. This method enhanced resolution at lower frequencies, providing a clearer understanding of the noise in that specific range. Through a series of experiments, wherein we varied the laser emission power (ranging from -10 to 10 dBm) and fiber length (30 km, 45 km, 55 km, and 80 km), we carefully scrutinized the resulting spectrum. During our investigation, we initially observed that the Lorentzian curve was not suitable for fitting the first few hundred hertz. Consequently, for frequencies up to 450 Hz, we adopted a Gaussian noise model. This model encompasses noise components originating from environmental factors, such as acoustic noise, temperature fluctuations, and vibrations [9], [10], as well as technical noise, like electronic noise, shot noise, or thermal noise [11]. For the remaining spectrum, we utilized a Lorentzian curve, which is commonly associated with phase noise resulting from spontaneous photon emission [1]. Our analysis yielded two additional noteworthy findings. Firstly, we identified a distinct feature likely connected to polarization mismatch in the frequency range of 800 Hz to 1200 Hz. Secondly, we observed excess noise, potentially linked to the beat of ASE (Amplified Spontaneous Emission) noise, spanning from 5 kHz to 100 kHz. This excess noise phenomenon was particularly noteworthy and deserving of further investigation. Fig. 3a depicts a typical result curve obtained using the proposed methodology: points A, B, C, and D represent relevant parts of the spectrum that will be used as a reference for the discussion. Firstly,

Brazilian Microwave and Optoelectronics Society-SBMO *received 17 Mar 2023; for review 19 Apr 2023; accepted 05 Oct 2023*
Brazilian Society of Electromagnetism-SBMag *ISSN 2179-1074*

a peak is observed in the experimental measurement at point A (Fig. 3a), indicating the presence of noise ranging from 0 to 190 Hz. The Gaussian distribution revealed good correlation in this part, so this frequency range was theoretically approximated using Eq. 4, depicted in further detail in Figure Fig. 3b) (green line/section). The contribution of this Gaussian low frequency noise is significant, and is estimated that environmental factors, such as mechanical vibrations and temperature variations, as well as factors arising from the device dynamics, are related in this region. Furthermore, $1/f$ noise type was also observed, as shown in Fig. 3b (red line over gray curve). Note that the $1/f$ noise extends to approximately 7 Hz (red trace) as shown in Fig. 3b. There is some fluctuation at point B (Fig. 3a). The careful polarization control (PC) adjustment is essential to decrease the fluctuations, which cause a difference in the experimental outcome from what is theoretically expected. Following that, in the region of point C, the experimental and theoretical curves have the best correlation (Fig. 3a). In this region, the fitting curve uses a Lorentzian approximation based on equation Eq. 3 and the measured noise extended to frequencies around 5 kHz (Fig. 3).

Finally, the region denoted by D (Fig. 3a), shows the beginning of a mismatch between the expected theoretical Lorentzian curve and the experimental measurement. It indicates the presence of noise at frequencies larger than 5 kHz in this example. This high frequency excess noise may be caused by

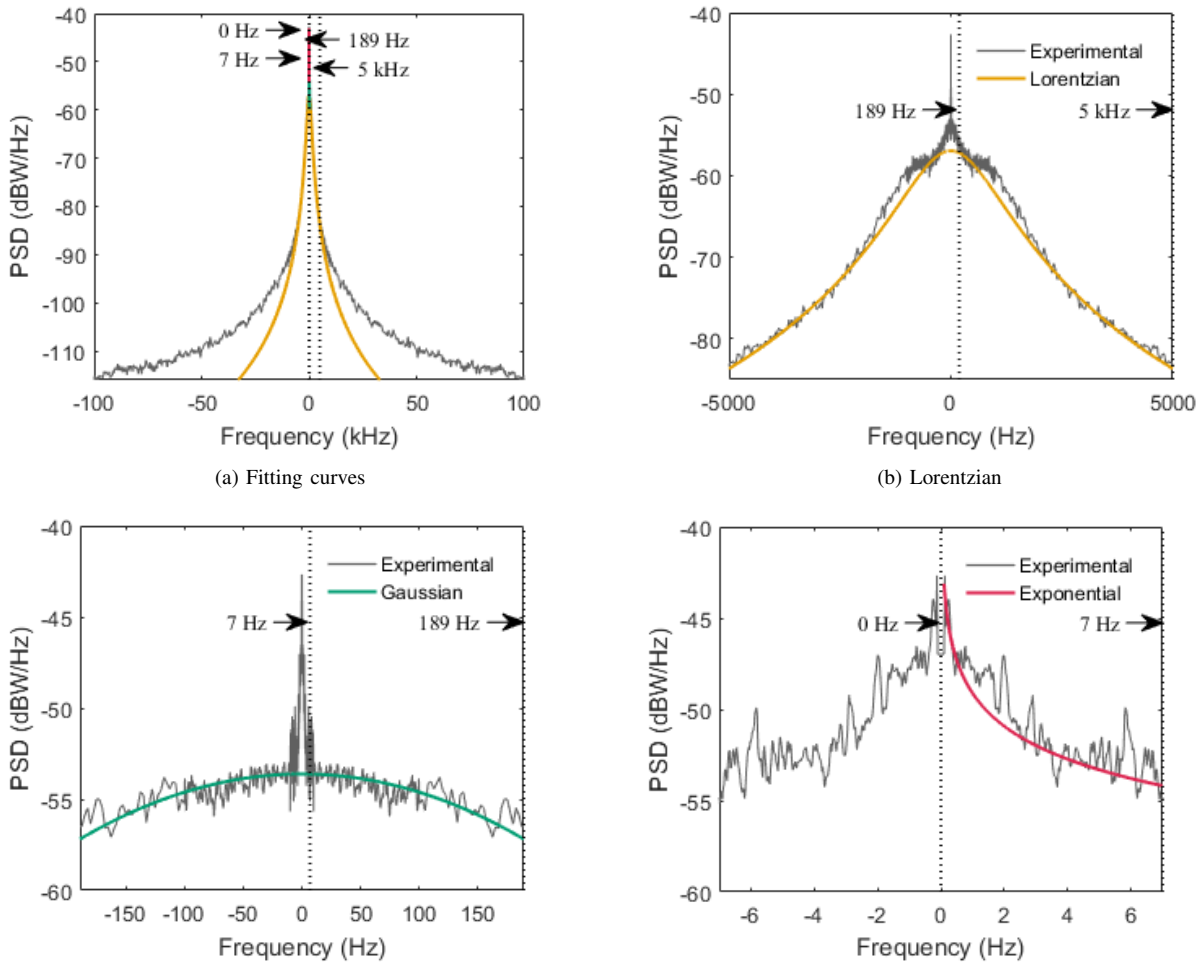

(a) Fitting curves

(b) Lorentzian

(c) Gaussian

(d) Exponential

Fig. 4. Using the best fitting curve for each part of the LFN spectrum.

ISSN 2179-1074

the beating of the spontaneous emission noise of the device when combined with its delayed replica. Anyway, an ideal laser should not have this kind of noise and the following results evince that this excess noise is related to a deterioration of the laser signal emission coherence.

The results shown in Fig. 4 are the best fitted curves for: the Lorentzian (Fig. 4a up to 100 kHz, and Fig. 4b up to 5 kHz); for the Gaussian fitting (Fig. 4c up to 189 Hz); and exponential fitting (Fig. 4d up to 7 Hz) related to the $1/f$ noise.

In Fig. 5 we show other results for 55 km fiber spool length with LD emitting 10 dBm and 2 dBm. For the 2 dBm laser power on Fig. 5b and Fig. 5d, the spectrum first exhibits the Gaussian profile (AB fit) and subsequently the Lorentzian profile (CE fit). Fig. 5a and Fig. 5c also show the laser running at higher power (+10 dBm), and the Gaussian noise is relatively smaller than 2 dBm curves. Another point to consider is the descent of the laser curve; by lowering the laser power, the spectral descent deviates significantly from the Lorentzian fit (point F), with a higher high frequency excess noise for the smaller power (circled regions). It is worth noting that as the laser power is reduced, a resonance at point X grows larger in amplitude. This resonance close to 2 kHz has an invariant frequency with power. Also, at 2 dBm power the circled region becomes almost flat as a result of higher excess noise.

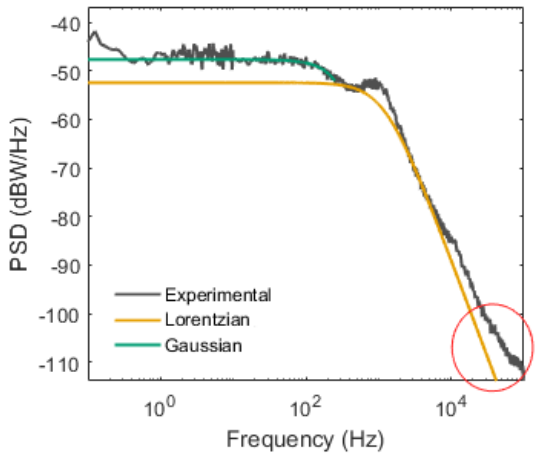

(a) RIO1 with 10 dBm laser power.

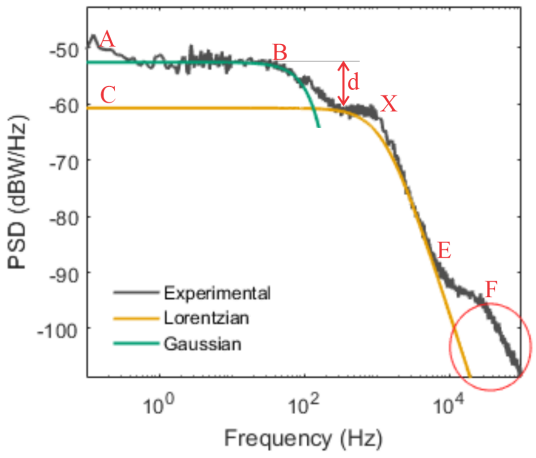

(b) RIO1 with 2 dBm laser power.

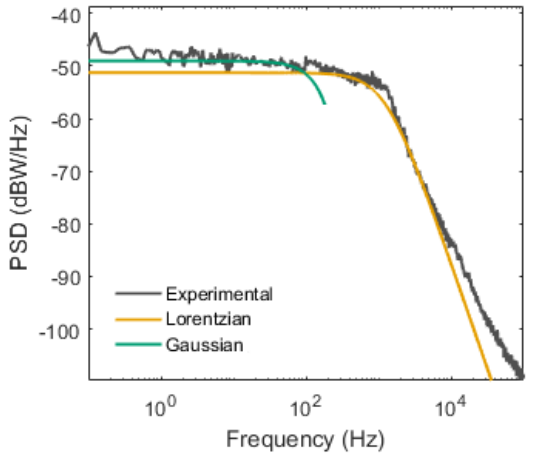

(c) RIO2 with 10 dBm laser power.

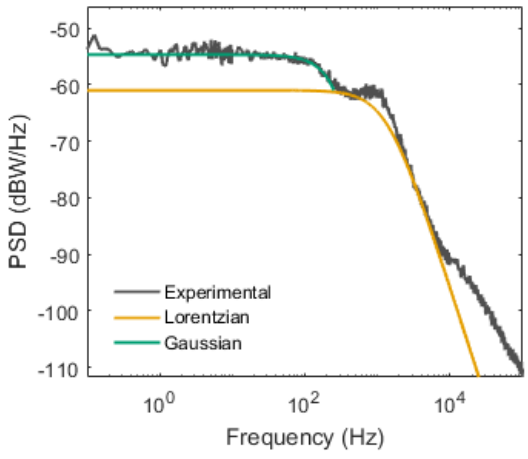

(d) RIO2 with 2 dBm laser power.

Fig. 5. PSD for 55 km fiber length.

ISSN 2179-1074

This occurs for all delay fiber length and both lasers (RIO1 and RIO2). In Fig. 5b it is possible to observe that the larger the distance d (for lower laser power), the greater the low-frequency noise contained in the Gaussian curve. As a result, the low frequency excess noise for low frequencies also grows as power decreases therefore low frequency excess noise just depend on the laser power not the frequency.

To evaluate the in(dependence) with the spool fiber length and the laser power emission, Fig. 6 should be considered. Fig. 6a demonstrates that the resonance point increases as the laser power decreases. Also, it gives some details on excess noise at high frequencies (increasing as emission powers decreases) and gaussian noise at low frequencies (increasing as emission powers decreases). Fig. 6b shows the laser PSD measurement with the 8dBm laser power and the delay fiber length ranging from 30km, 45km, 55km and 80km. It can be seen that PSD measurement does not present considerable variations. However, with the fiber length 30km (or less), the PSD exhibit excessive oscillations, causing some inaccuracy in the measurements. When the fiber length is reduced to 1000m, the PSD curve becomes almost unacceptable because the delay time is reduced due to the short fiber length and the phase difference between two arms is decreasing. The PSD measurement is not possible in this case.

By using the LREN factor defined in Eq. 8(see data at Appendix), Fig. 7a (laser RIO1) and Fig. 7b (laser RIO2) show the relative excess noises of both lasers under test versus their optical output power; both results show that the Laser relative excess noise (LREN) decreases as the laser power increases. Since the laser linewidth decreases with the laser power, the LREN is related to the laser emission coherence. An ideal laser should have its PSD spectrum entirely fitted as a Lorentzian waveform. So, the ideal laser would have $LREN = 0$. If the laser could support a stronger power, the tendency of the curves of Fig. 7 shows that a power of 17 dBm might approach the laser as an ideal Lorentzian laser.

In this study, we examined the spectral noise characteristics of an Integrated External Cavity laser (IECL) manufactured by Redfern Integrated Optics Inc. (RIO). This particular laser demonstrates a low noise level, with a linewidth below 3 kHz. There is no description of the state of either of these two lasers, including usage history or manufacture imperfections because they are both old and have been in use for a long time. However, it is feasible to infer from Fig. 7b that the laser RIO2 behaves more

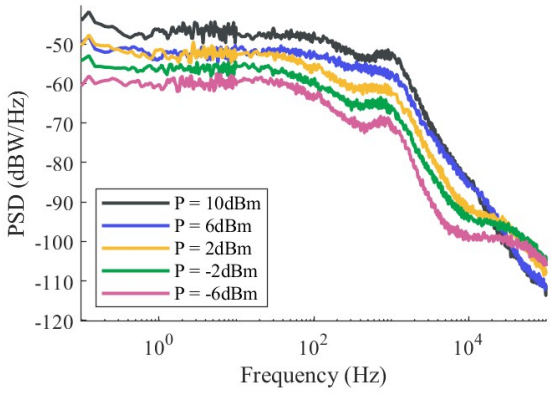

(a) The PSD in relation to laser power for the RIO1 laser with a fiber length of 55km.

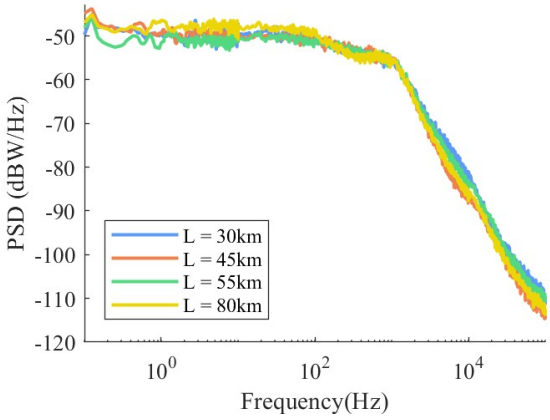

(b) PSD comparison for various fiber lengths and 10dBm laser power (RIO1 laser).

Fig. 6. PSD comparison showing the (in)dependence with laser output power and spool fiber length.

ISSN 2179-1074

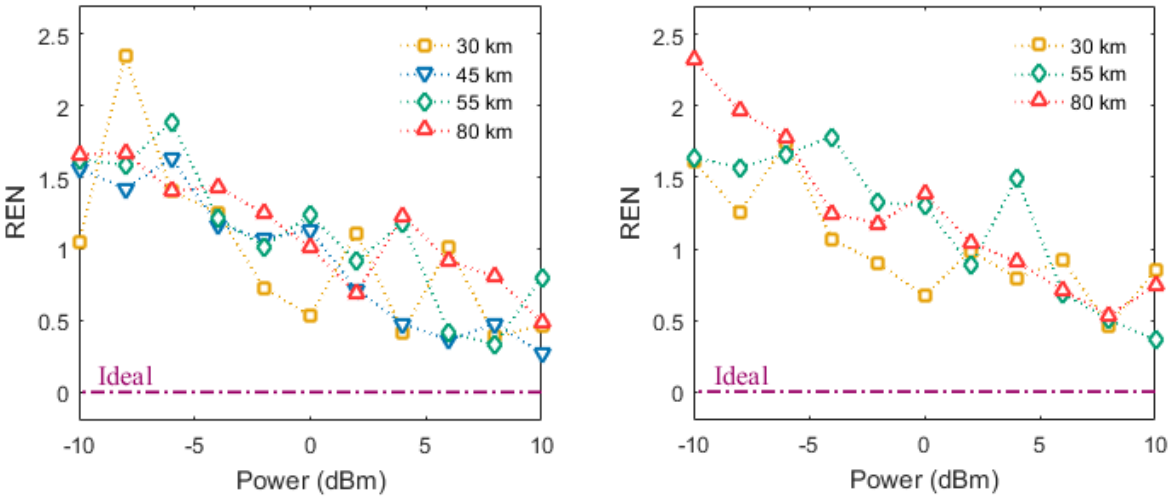

(a) RIO1 (b) RIO2

Fig. 7. Laser relative excess noise (LREN) in terms of power.

consistently than RIO1, and the LREN of the RIO2 values is lower than RIO1. Fig. 7a demonstrates that the LREN of the RIO2 tends to decline as laser power rises, but the RIO1 exhibits some oscillations as power varies.

Also, note that the long arm spans of 55 and 80 km give better results than 35 km, as discussed before. However, considering a laser linewidth lower than 5 kHz for the tested laser, a much longer fiber span would be necessary to completely break the coherence of the two signals of the UMZI. This is due to several factors, such as Phase Noise Accumulation: the longer arm spans allow for a greater accumulation of phase noise along the optical path. Phase noise can result from various factors, such as fiber birefringence, temperature fluctuations, and laser frequency instability. With longer arm spans, the phase noise has more time to accumulate, leading to a larger phase noise contribution to the linewidth. Another factor is the Interference Pattern Sensitivity: in an interferometer the interference pattern is highly sensitive to phase differences between the two arms. Longer arm spans result in a larger phase difference between the arms, leading to more pronounced interference fringes. This increased sensitivity enables better resolution of the linewidth. Polarization Effects: fiber birefringence, which can cause polarization variations, is a common source of linewidth broadening. Longer arm spans provide a larger physical distance for the polarization state to evolve, allowing for better characterization and compensation of polarization effects. By implementing techniques to monitor and stabilize the polarization, the linewidth measurement accuracy can be improved. Overall, the longer arm spans in the unbalanced Mach-Zehnder interferometer allow for better characterization and compensation of phase noise, polarization effects, leading to improved linewidth measurement results compared to shorter spans.

IV. Conclusion

The methodology proposed here uses the phase fluctuations and excess noise in a coherent optical field to evaluate the optical source noises. The LD $1/f$, Gaussian, Lorentzian, and excess noises were theoretically and experimentally evaluated, and the non-destructive method was used to determine the LREN factor of two lasers with different fiber lengths. This non-destructive technique can be used

ISSN 2179-1074

to measure laser noises with higher accuracy while providing an evaluation of the laser noises when the laser has a linewidth below 10 kHz. Note in Fig. 7 that the variation is lower at 80 km delay (red triangles) in relation to the 30 km delay (yellow squares). This variation is due to the difficulty of manually optimize the polarization of the long and short UMZI arms signals. Indeed, the noise variation due to polarization mismatch, shown by X region in Fig. 5b, is higher for lower fiber spool lengths. An automatic polarization control could improve the technique presented here.

REFERENCES

[1] L. Riuttanen, P. Kivisaari, H. Nykänen, O. Svensk, S. Suihkonen, J. Oksanen, J. Tulkki, and M. Sopanen, "Diffusion injected multi-quantum well light-emitting diode structure," *Applied Physics Letters*, vol. 104, no. 8, p. 081102, 2014.

[2] Y. Liu, S. Zhao, S. Yang, Y. Li, and R. Qiang, "Markov process based reliability model for laser diodes in space radiation environment," *Microelectronics Reliability*, vol. 54, no. 12, pp. 2735–2739, 2014.

[3] J. Yang, B. Yang, W. Zhang, Y. Zhao, Z. Du, Y. Zeng, J. Zhou, H. Gui, L. lu, and B. Yu, "Numerical simulation of phase modulation method used as high sensitive self-mixing vibrometry in vertical-cavity surface-emitting laser," *Optik*, vol. 124, no. 23, pp. 6017–6019, 2013.

[4] J. Guan, S. Guo, J. Wang, M. Tao, J. Cao, and F. Gao, "Analysis of origin of measured 1/f noise in high-power semiconductor laser diodes far below threshold current," *Microelectronics Reliability*, vol. 59, pp. 55–59, 2016.

[5] X. Zhang, S. Thapa, and N. Dutta, "All-optical xor gates based on dual semiconductor optical amplifiers," *Cogent Physics*, vol. 6, 08 2019.

[6] E. Conforti, M. Rodigheri, T. Sutili, and F. Galdieri, "Acoustical and 1/f noises in narrow linewidth lasers," *Optics Communications*, vol. 476, p. 126286, 07 2020.

[7] T. Sutili, R. C. Figueiredo, and E. Conforti, "Laser linewidth and phase noise evaluation using heterodyne offline signal processing," *Journal of Lightwave Technology*, vol. 34, no. 21, pp. 4933–4940, 2016.

[8] K. Kikuchi, T. Okoshi, M. Nagamatsu, and N. Henmi, "Degradation of bit-error rate in coherent optical communications due to spectral spread of the transmitter and the local oscillator," *Journal of Lightwave Technology*, vol. 2, no. 6, pp. 1024–1033, 1984.

[9] D. Welch, "A brief history of high-power semiconductor lasers," *IEEE Journal of Selected Topics in QuantumElectronics*, vol. 6, no. 6, pp. 1470–1477, 2000.

[10] S. Pralgauskaitė, V. Palenskis, J. Matukas, J. Glemža, G. Muliuk, B. Šaulys, and A. Trinkūnas, "Reliability investigation of light-emitting diodes via low frequency noise characteristics," *Microelectronics Reliability*, vol. 55, no. 1, pp. 52–61, 2015.

[11] L. Mercer, "1/f frequency noise effects on self-heterodyne linewidth measurements," *Journal of Lightwave Technology*, vol. 9, no. 4, pp. 485–493, 1991.

[12] A. Dandridge and H. Taylor, "Correlation of low-frequency intensity and frequency fluctuations in gaalas lasers," *IEEE Transactions on Microwave Theory and Techniques*, vol. 30, no. 10, pp. 1726–1738, 1982.

[13] O. Llopis, S. Azaizia, K. Saleh, A. A. Slimane, and A. Fernandez, "Photodiode 1/f noise and other types of less known baseband noises in optical telecommunications devices," in *2013 22nd International Conference on Noise and Fluctuations (ICNF)*, pp. 1–4, 2013.

[14] S. Mahdi, "The power spectral density of 1noise in a tunable diode laser at different temperatures," *Journal of Optics*, vol. 47, 09 2017.

[15] D. Eliyahu, D. Seidel, and L. Maleki, "Rf amplitude and phase-noise reduction of an optical link and an opto-electronic oscillator," *IEEE Transactions on Microwave Theory and Techniques*, vol. 56, no. 2, pp. 449–456, 2008.

[16] Z. Celik-Butler and T. Hsiang, "Determination of si-sio/sub 2/ interface trap density by 1/f noise measurements," *IEEE Transactions on Electron Devices*, vol. 35, no. 10, pp. 1651–1655, 1988.

[17] D. M. Fleetwood and J. H. Scofield, "Evidence that similar point defects cause 1/f noise and radiation-induced-hole trapping in metal-oxide-semiconductor transistors," *Phys. Rev. Lett.*, vol. 64, pp. 579–582, Jan 1990.

[18] L. Hasse, S. Babicz, L. Kaczmarek, J. Smulko, and V. Sedlakova, "Quality assessment of zno-based varistors by 1/f noise," *Microelectronics Reliability*, vol. 54, p. 192–199, 01 2014.

[19] H. Zhu, K. Liu, C. Xiong, S. Feng, and C. Guo, "The effect of external stress on the properties of algaas/gaas single quantum well laser diodes," *Microelectronics Reliability*, vol. 55, 11 2014.

received 17 Mar 2023; for review 19 Apr 2023; accepted 05 Oct 2023

ISSN 2179-1074

[20] M. Fukuda, F. Kano, T. Kurosaki, and J. Yoshida, "Reliability and degradation behavior of highly coherent 1.55 mu m long-cavity multiple quantum well (mqw) dfb lasers," *Journal of Lightwave Technology*, vol. 10, no. 8, pp. 1097–1104, 1992.

[21] M. Fukuda, T. Hirono, T. Kurosaki, and F. Kano, "1/f noise behavior in semiconductor laser degradation," *IEEE Photonics Technology Letters*, vol. 5, no. 10, pp. 1165–1167, 1993.

[22] G. P. Agrawal, *Fiber-Optic Communication Systems*, 3rd ed. John Wiley & Sons, 2002.

[23] R. Ramaswami and K. N. Sivarajan, *Optical Networks: A Practical Perspective*, 2nd ed. Elsevier Science, 2002.

[24] G. P. Agrawal and N. K. Dutta, *Semiconductor Lasers*, 2nd ed. Van Nostrand Reinhold, 1993.

[25] A. van der Ziel, "Noise in solid-state devices and lasers," *Proceedings of the IEEE*, vol. 58, no. 8, pp. 1178–1206, 1970.

[26] R. Paschotta, "Noise in laser technology," *Optik & Photonik*, vol. 4, no. 2, pp. 48–50, 2009.

[27] A. E. Siegman, *Lasers*. University Science Books, 1986.

[28] C. Henry, "Phase noise in semiconductor lasers," *Journal of Lightwave Technology*, vol. 4, no. 3, pp. 298–311, 1986.

[29] F. Grüneis, "1/f noise due to atomic diffusion of impurity centers in semiconductors," *Fluctuation and Noise Letters*, vol. 01, no. 04, pp. L197–L220, 2001.

[30] J. Matukas, V. Palenskis, C. Pavasaris, E. Sermuksnis, J. Vysniauskas, S. Pralgauskaitė, G. Letal, S. Smetona, J. Simmons, and R. Sobiestijanskas, "Optical and electrical characteristics of ingaasp mqw bh dfb laser diodes," *Materials Science Forum*, vol. 384, p. 91, 01 2002.

[31] R. Fronen and F. Hooge, "1/f noise in a p-i-n diode and in a diode laser below threshold," *Solid-State Electronics*, vol. 34, no. 9, pp. 977–982, 1991.

[32] R. Fronen and L. Vandamme, "Low-frequency intensity noise in semiconductor lasers," *IEEE Journal of Quantum Electronics*, vol. 24, no. 5, pp. 724–736, 1988.

[33] F. Hooge, "1/f noise sources," *IEEE Transactions on Electron Devices*, vol. 41, no. 11, pp. 1926–1935, 1994.

[34] M. Fukuda, T. Hirono, T. Kurosaki, and F. Kano, "Correlation between 1/f noise and semiconductor laser degradation," *Quality and Reliability Engineering International*, vol. 10, no. 4, pp. 351–353, 1994.

[35] M. Fukuda and G. Iwane, "Degradation of active region in ingaasp/inp buried heterostructure lasers," *Journal of Applied Physics*, vol. 58, no. 8, pp. 2932–2936, 1985.

[36] ——, "Correlation between degradation and device characteristic changes in ingaasp/inp buried heterostructure lasers," *Journal of Applied Physics*, vol. 59, no. 4, pp. 1031–1037, 1986.

[37] A. Ali and D. Abdul-Wahid, "Analysis of self-homodyne and delayed self-heterodyne detections for tunable laser source linewidth measurements," *IOSR Journal of Engineering (IOSRJEN)*, vol. 2, pp. 1–6, 10 2012.

[38] Z. Bai, Z. Zhao, Y. Qi, J. Ding, S. Li, X. Yan, Y. Wang, and Z. Lu, "Narrow-linewidth laser linewidth measurement technology," *Frontiers in Physics*, vol. 9, 11 2021.

[39] F. J. Galdieri, T. Sutili, N. Melnikoff, A. C. Bordonalli, and E. Conforti, "Influence of exterior acoustic noise on narrow linewidth laser measurements using self-homodyne optical fiber interferometer," *Optik*, vol. 204, p. 164101, 2020.

[40] H. Ludvigsen, M. Tossavainen, and M. Kaivola, "Laser linewidth measurements using self-homodyne detection with short delay," *Optics Communications*, vol. 155, no. 1, pp. 180–186, 1998.

[41] A. L. Schawlow and C. H. Townes, "Infrared and optical masers," *Phys. Rev.*, vol. 112, pp. 1940–1949, Dec 1958.

APPENDIX

Table I to Table VII contains the three main regions of the PSD spectrum and LREN factor calculated for two lasers (RIO1 and RIO2) with different fiber lengths. RIO is a narrow linewidth laser (linewidth less than 4 kHz) with an external cavity and 1550 nm center wavelength. The LREN factor is assessed by the Eq. 8. It demonstrates that as the laser power is reduced, the LREN increases. A resonance point discussed above induces strongly variations in this quantity.

ACKNOWLEDGMENTS

Authors would like to thank Brazilian agencies *São Paulo Research Foundation* (FAPESP – grants 22/11596-0, 21/11380-5, 21/06569-1 and 20/08362-2), and *National Council for Scientific and Technological Development* (CNPq – grants 141342/2019-6, 303595/2021-3 and 305104/2021-7).

  ISSN 2179-1074

TABLE I. Algorithm calculated powers for laser RIO1 and $L = 80$ km.

P (dBm)	P_T (mW)	P_L (mW)	P_G (mW)	P_E (mW)	$LREN$
10	9.866	6.621	1.441	1.805	0.49
8	6.208	3.44	1.692	1.076	0.805
6	3.925	2.049	0.948	0.928	0.916
4	2.475	1.11	0.782	0.583	1.23
2	1.553	0.92	0.468	0.165	0.688
0	0.987	0.491	0.294	0.201	1.009
-2	0.62	0.276	0.214	0.13	1.246
-4	0.392	0.161	0.143	0.088	1.434
-6	0.247	0.103	0.062	0.082	1.403
-8	0.156	0.058	0.041	0.056	1.672
-10	0.097	0.037	0.029	0.032	1.659

TABLE II. Algorithm calculated powers for laser RIO1 and $L = 55$ km.

P (dBm)	P_T (mW)	P_L (mW)	P_G (mW)	P_E (mW)	$LREN$
10	9.818	5.448	2.327	2.042	0.802
8	6.204	4.646	0.717	0.841	0.335
6	3.911	2.775	0.583	0.553	0.41
4	2.465	1.129	0.578	0.758	1.184
2	1.557	0.814	0.334	0.41	0.914
0	0.983	0.44	0.284	0.259	1.234
-2	0.62	0.307	0.152	0.16	1.017
-4	0.392	0.177	0.093	0.122	1.215
-6	0.247	0.086	0.075	0.087	1.888
-8	0.156	0.06	0.047	0.049	1.586
-10	0.098	0.037	0.029	0.032	1.624

TABLE III. Algorithm calculated powers for laser RIO1 and $L = 45$ km.

P (dBm)	P_T (mW)	P_L (mW)	P_G (mW)	P_E (mW)	$LREN$
10	9.821	7.717	1.403	0.701	0.273
8	6.201	4.192	1.331	0.677	0.479
6	3.922	2.879	0.862	0.181	0.362
4	2.475	1.675	0.464	0.337	0.478
2	1.562	0.911	0.393	0.258	0.715
0	0.98	0.46	0.319	0.202	1.131
-2	0.621	0.3	0.212	0.109	1.072
-4	0.392	0.181	0.123	0.089	1.169
-6	0.246	0.094	0.106	0.047	1.631
-8	0.156	0.065	0.055	0.037	1.42
-10	0.099	0.039	0.037	0.023	1.561

TABLE IV. Algorithm calculated powers for laser RIO1 and $L = 30$ km.

P (dBm)	P_T (mW)	P_L (mW)	P_G (mW)	P_E (mW)	$LREN$
10	9.837	6.709	1.543	1.585	0.466
8	6.213	4.48	0.77	0.963	0.387
6	3.732	1.855	0.327	1.55	1.012
4	2.454	1.729	0.365	0.36	0.42
2	1.548	0.733	0.297	0.518	1.112
0	0.986	0.643	0.189	0.154	0.533
-2	0.617	0.357	0.138	0.123	0.729
-4	0.384	0.171	0.117	0.097	1.252
-6	0.246	0.102	0.058	0.085	1.404
-8	0.155	0.046	0.06	0.049	2.347
-10	0.097	0.047	0.037	0.013	1.048

Brazilian Microwave and Optoelectronics Society-SBMO *received 17 Mar 2023; for review 19 Apr 2023; accepted 05 Oct 2023*
Brazilian Society of Electromagnetism-SBMag *ISSN 2179-1074*

TABLE V. Algorithm calculated powers for laser RIO2 and $L = 80$ km.

P (dBm)	P_T (mW)	P_L (mW)	P_G (mW)	P_E (mW)	$LREN$
10	9.853	5.66	1.968	2.224	0.741
8	6.212	4.046	1.104	1.062	0.535
6	3.921	2.293	0.968	0.66	0.71
4	2.467	1.293	0.605	0.569	0.909
2	1.561	0.763	0.449	0.349	1.047
0	0.983	0.412	0.327	0.244	1.383
-2	0.622	0.286	0.171	0.165	1.177
-4	0.392	0.174	0.13	0.087	1.249
-6	0.247	0.089	0.071	0.087	1.777
-8	0.156	0.053	0.057	0.046	1.966
-10	0.098	0.03	0.029	0.04	2.325

TABLE VI. Algorithm calculated powers for laser RIO2 and $L = 55$ km.

P (dBm)	P_T (mW)	P_L (mW)	P_G (mW)	P_E (mW)	$LREN$
10	9.822	7.207	0.298	2.317	0.363
8	6.206	4.132	1.312	0.762	0.502
6	3.906	2.312	0.896	0.698	0.69
4	2.449	0.983	0.664	0.802	1.492
2	1.56	0.829	0.444	0.287	0.882
0	0.981	0.425	0.317	0.239	1.308
-2	0.621	0.267	0.216	0.138	1.321
-4	0.391	0.14	0.111	0.14	1.784
-6	0.247	0.093	0.084	0.071	1.664
-8	0.156	0.061	0.055	0.04	1.571
-10	0.099	0.037	0.029	0.032	1.639

TABLE VII. Algorithm calculated powers for laser RIO2 and $L = 30$ km.

P (dBm)	P_T (mW)	P_L (mW)	P_G (mW)	P_E (mW)	$LREN$
10	9.74	5.274	2.087	2.379	0.847
8	6.081	4.16	0.763	1.158	0.462
6	3.908	2.036	1.016	0.857	0.92
4	2.476	1.378	0.493	0.605	0.796
2	1.554	0.782	0.402	0.37	0.986
0	0.985	0.59	0.217	0.179	0.671
-2	0.617	0.325	0.162	0.13	0.9
-4	0.39	0.189	0.099	0.103	1.069
-6	0.245	0.089	0.079	0.076	1.74
-8	0.156	0.069	0.037	0.05	1.254
-10	0.099	0.038	0.026	0.035	1.613

Brazilian Microwave and Optoelectronics Society-SBMO *received 17 Mar 2023; for review 19 Apr 2023; accepted 05 Oct 2023*
Brazilian Society of Electromagnetism-SBMag *ISSN 2179-1074*